APPENDIX B: Cask Response to Mechanical and Thermal Loads

This page is intentionally blank

Appendix B

Cask Response to Mechanical and Thermal Loads

B.1 Purpose and Scope

The purpose of Appendix B is to provide a more detailed analysis and discussion of the response of the Multi-Purpose Canister (MPC) to the mechanical and thermal load events that could occur as a result of the sequence of actions that occur during the handling and transfer process, and conditions that could be experienced during storage. This Appendix provides information in addition to that presented in the main body of the PRA report.

The scope of this Appendix encompasses the range of possible responses to mechanical and thermal load scenarios/events that could pose a challenge to the MPC. It is assumed that the MPC is built as designed, so fabrication errors are not included in the scope, and that materials are procured and components constructed to the quality standards set forth in the SAR (Reference B.1) and the ASME Boiler and Pressure Vessel Code. Although weld metal typically has a higher strength than base metal, it is generally known that weld-deposited austenitic stainless steels, while very ductile, have a tendency to be less ductile than the wrought product. At the strain levels that may be encountered in beyond design basis events, such as severe drop impacts, this potential reduction in ductility of the deposited weld metal is important, and therefore is considered in evaluating the structural integrity of the MPC.

B.1.1 MPC description

In the HI-STORM dry storage cask system, the MPC acts as the confinement boundary. A drawing of the major welds of the MPC and its components is shown in Figure B.1. The MPC is made entirely of austenitic stainless steel. The cylindrical shell is constructed from one circumferential and four axial seam welds that join the 1.27 cm (0.5 in.) thick plates. The 2 axial welds on each side of the MPC are slightly offset at the circumferential weld. This cylindrical shell is then welded to a 6.35 cm (2.5 inch) thick baseplate. The MPC seam welds, and shell to baseplate weld are then subjected to a hydrostatic test of 0.86 MPa (125 psi). The welds are fabricated per ASME Code, Section III, Subsection NB specifications. These are full-penetration submerged arc welds which undergo dye-penetrant (PT), radiographic (RT) or ultrasonic (UT) examinations per ASME Code, Section V (Articles 2, 6, or 5 respectively) examinations. The welds' acceptance criteria are those in Articles NB-5320, NB-5350, and NB-5360 for PT, RT and UT examinations, respectively. They are not post-weld heat treated to remove residual stresses.

After the cask is loaded with fuel, the MPC lid is welded to the shell. This 1.9 cm (0.75 in) thick weld undergoes PT examinations after the root, intermediate and final weld passes. These lid welds are performed using the tungsten-inert-gas (TIG) process.

The vent and drain ports used for drying and inerting are welded closed with cover plates. These welds undergo a final PT examination and leak test. The MPC lid-to-shell weld and the vent and drain cover plate welds form the primary seal to the MPC lid. A closure ring is then placed on the MPC lid and welded to the shell and lid to form a redundant cask seal. These vent and drain cover plate welds and the ring welds are also made using the TIG process. This design ensures the cask environment is separated from the outside atmosphere by two independent lid welds.

The MPC lid welds were not considered in the MPC failure assessments for the following reasons:

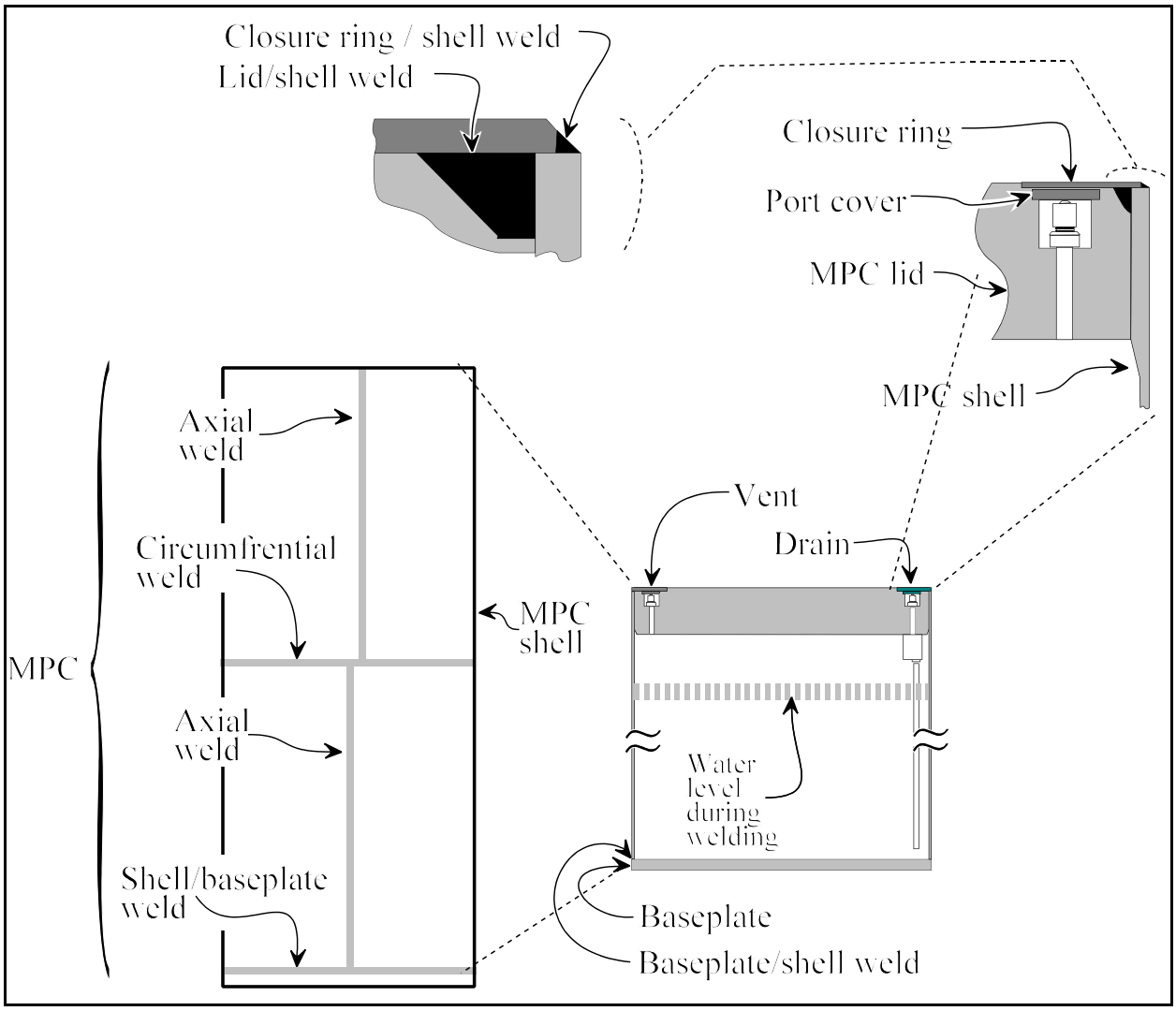

Figure B.1 Major Welds of the MPC

1. The TIG process used on the lid generally produces a tougher weld than the SA weld used in the shell of the MPC.

2. The redundancy of the lid design requires at least two welds to fail in order for MPC confinement to be compromised.

3. The applied stresses at these locations are significantly less than the stresses in the MPC shell for all events analyzed.

B.1.2 MPC Stresses

Mechanical loads

In the PRA several mechanical impact accident scenarios were considered:

1. Transfer Cask Drop onto Concrete Floor: This is a handling accident in which the transfer overpack (HI-TRAC) with the MPC inside is dropped on a concrete floor from various heights.

2. Transfer Cask Drop onto Storage Cask: This is a handling accident in which the transfer overpack (HI-TRAC) with the MPC inside is being lowered from a height of up to 24.4 m (80 ft) and falls on the storage overpack.

3. MPC Drop: This is also a handling accident in which the MPC falls from a height of 5.8 m (19 ft) when being lowered from the transfer overpack (HI-TRAC) to the storage overpack (HI-STORM).

4. Storage Cask Drop: This is a transport accident in which the storage overpack (HI-STORM) with the MPC inside is dropped from a height of 0.30 m (1 ft) on concrete, gravel and asphalt.

5. Storage Cask Tip-over: This is a storage accident in which the storage cask with the MPC inside is tipped over on the concrete storage pad.

The analyses used to calculate the MPC stresses for these events are described in Appendix A of this report.

The thermal analyses described in Section 4.2 indicated that steady state conditions within the MPC under normal conditions would be attained prior to the initiation of the various handling and transfer events that move fuel out to the storage pad. These steady state conditions are an internal pressure of 0.564 MPa (82 psi) with an MPC temperature that varies axially from 73°C (163°F) to 180°C (356°F).

It was assumed that the MPC is under normal steady state conditions during the mechanical impact scenarios listed above. In addition, all of the fuel is assumed to be intact during these events. Fuel cladding failure would cause the internal pressure of the MPC to increase. If a mechanical impact event did cause fuel cladding failure, the resulting increase in pressure would not occur during the accident scenario. The increase in internal pressure due to fuel cladding failure would be a result of the mechanical loading, but because of the extremely short duration of the impact, it would not effect the MPC internal pressure until after the mechanical loading is complete.

Thermal loads

Only two thermal accident scenarios are considered in this PRA:

1. Storage Cask External Fire: This is a storage accident in which the storage overpack (HI-STORM) with the MPC inside is exposed to an external fire resulting from a Gulfstream IV aircraft crash. A credible fire scenario will be less than 30 minutes. However, the analysis was performed for a fire duration of 3 hours.

2. Storage Cask Vent Blockage: This is a storage accident in which the cooling vents of the storage overpack (HI-STORM) become completely blocked for a period of 20 years.

Under thermal loads the only significant MPC stresses are due to internal pressure. Membrane stresses were calculated using the classical shell theory equations for pressurized cylinders:

$$\sigma_{axial} \equiv \frac{P \bullet r}{2 \bullet t} \tag{B.1}$$

$$\sigma_{hoop} \equiv \frac{P \bullet r}{t} \tag{B.2}$$

where: σ_{axial} = axial stress in psi
σ_{hoop} = hoop stress in psi
P = internal pressure in psi
r = MPC internal radius in inches (= 33.6875 in. or 85.5663 cm)
t = MPC wall thickness in inches (= 0.5 in or 1.27 cm)

The initial steady-state pressure of the MPC is 0.565 MPa (82 psi). Using Equations B.1 and B.2, the resulting axial and hoop stresses are 19.05 MPa (2,762 psi) and 38.1 MPa (5,525 psi), respectively.

The highest stress due to internal pressure loads occurs at the shell to baseplate connection. Section 3.4.4.3.1.2 of Reference B.1 analyzed the MPC stresses at various locations due to an internal pressure of 0.69 MPa (100 psi). These results showed that the total (membrane plus bending) stress at the MPC shell-to-baseplate connection was 303 MPa (43,986 psi). The axial membrane stress at this pressure is 23.6 MPa (3,419 psi). The difference in these values gives the bending stress acting on the shell-to-baseplate weld as 280 MPa (40,567 psi). The total stress at other pressures was assumed to be directly proportional to those at 0.69 MPa (100 psi). Therefore, at a pressure of 0.565 MPa (82 psi), the total stress at this location is only 248.7 MPa (36,068 psi). Subtracting the axial membrane stress of 19.05 MPa (2,762 psi) gives a bending stress of 229.6 MPa (33,306 psi).

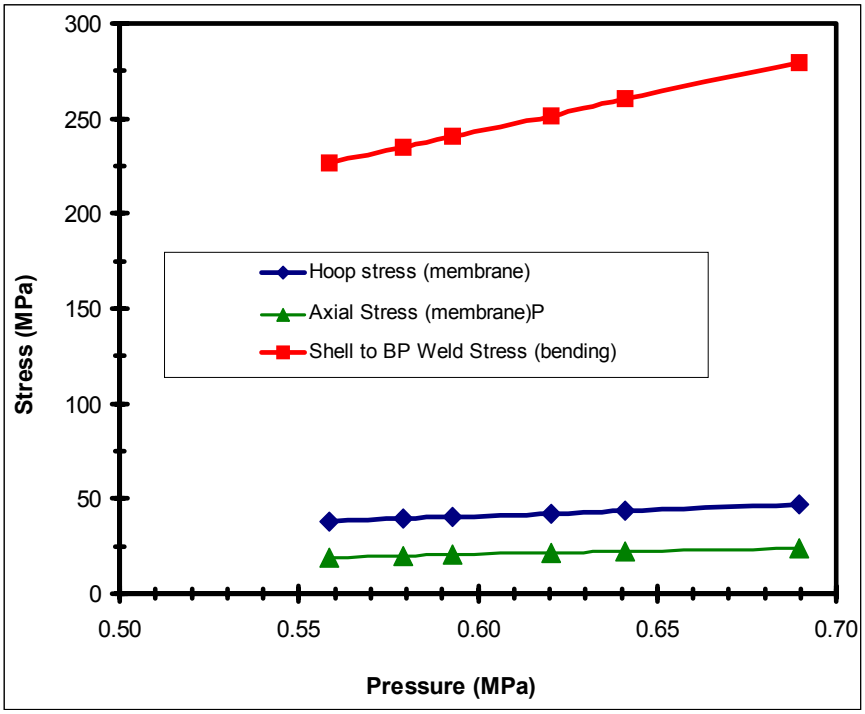

Figure B.2: MPC Stresses as a Function of Internal Pressure

The thermal accident scenarios listed above cause the MPC temperature and internal pressure to increase. A description of the thermal analyses used to calculate the new MPC temperatures and pressures are described in Section 4.2.1.1, "Heatup Model," of the Dry Cask Storage PRA report. Figure B.2 shows the increase in axial membrane, hoop membrane, and shell to baseplate bending stress with increasing pressure.

B.1.3 MPC Failure Mechanisms

The following failure mechanisms were postulated for the MPC under mechanical and thermal loads:

1. Weld Fracture,
2. Exceeding the Limit Load, and
3. Creep Rupture.

All three failure mechanisms were considered for thermal events, while only weld fracture was postulated for mechanical impacts. For the purposes of this PRA, failure mechanisms are assumed to be independent. The probability of MPC failure is given as the sum of the failure probabilities from each failure mechanism.

The failure analysis for weld fracture was based on test data of Type 308 weld deposited stainless steel specimens, and specimens taken from the weldments of Process Water Piping of nuclear production reactors constructed in the 1950's at the Savannah River Site. The mean and standard deviation of the failure strain data was calculated and adjusted for the effects of strain rate, temperature and state of stress. These results were used directly to determine the probability of weld fracture given the maximum strain calculated for each impact event.

Failure analyses for limit load and creep rupture were conducted differently from the failure analysis for weld fracture due to mechanical loads. Failure models for limit load and creep rupture were created in a spreadsheet with an add-on module called @RISK® (from www.palisade.com). This module allows Monte Carlo simulations to be run in the spreadsheet by allowing values in the spreadsheet cells to be sampled from statistical distributions. The user specifies which cells are considered outputs, and the number of iterations to perform. For each iteration, the program samples values from all cells in which a statistical distribution is specified, recalculates the entire spreadsheet, and records the values in the specified output cells. The distribution of output values can then be plotted and analyzed.

Separate spreadsheets were developed for the limit load and creep rupture mechanisms. The entire MPC was modeled through a series of spreadsheets representing the different parts of the MPC. Input cells for the spreadsheets defined the material properties, flaw parameters, and applied stresses. The only inputs not sampled from statistical distributions were the applied stresses on the MPC. The statistical distributions used to describe the material properties and flaw parameters are described in Section B.1.5. The specific inputs and calculations performed in each failure model spreadsheet are described in detail in Sections B.1.6 and B.1.7. The spreadsheet cell specified as output identifies each iteration as either an MPC success or failure. This process is repeated many times in a Monte-Carlo simulation. The probability of failure was calculated by dividing the total number of MPC failures by the total number of iterations performed.

The failure models used in this PRA do not attempt to predict the hole size in the MPC for a given failure probability. Any failure is assumed to create a hole in the MPC large enough to allow the particles and gases within the MPC to be released. This assumption was made because of the difficulty inherent in trying to predict the equivalent hole size produced from a particular MPC failure mode.

B.1.4 Weld Fracture due to Mechanical Loads

Appendix A evaluated the structural response of the MPC for various end drop scenarios. The objective was to determine the maximum effective plastic strain on the MPC confinement boundary for each of these scenarios. The analyses showed that the most highly stressed regions of the MPC are near the base of the cylindrical shell and in the weld joining the shell to the 2.5 inch thick baseplate.

To determine if confinement boundary integrity is compromised, the maximum effective plastic strain (EPS) in the MPC must be compared to an appropriate strain failure criterion. For a valid comparison, the conditions under which the maximum effective plastic strain is calculated, and the conditions under which the failure strain limit is measured, should be consistent. The comparison, therefore, must account for how the strain is measured, as well as the effects of strain rate, temperature and state of stress. It is the objective of this section to establish a valid basis for this comparison, and to estimate the probability of exceeding the failure strain limit for a given drop event.

Strain Measure

The LS-DYNA computer program used in the analysis for Appendix A to calculate MPC stresses and strains considers the reduction in cross-sectional area of the finite elements in the computation of stress within the element. Therefore, the program expects the user to input a true stress strain curve, which, by definition, considers the reduction in area in the computation of stress. Since the calculation of effective plastic strain within LS-DYNA is based on true strain, the failure criterion should also be based on a true strain measure.

The true strain at failure is calculated from the reduction in area (RA) within the necked-down region of a failed specimen as given in Equation (B.3) below.

$$\varepsilon_t = \ell n\left(\frac{1}{1 - RA}\right) \tag{B.3}$$

where, ε_t = true strain of failure, and
RA = reduction in area

The MPC shell is fabricated from Type 304 stainless steel. (See discussion in Section A.4.3.) Based on a review of References B.15 and B.16, a typical RA of Type 304 stainless steel at room temperature and static loading is 70%. Substituting RA equal to 0.70 into Equation(B.3) the true strain at failure is 1.20 in/in or 120% strain. This value is consistent with typical true stress strain curves that can be found in Reference B.17 for Type 304 stainless steel.

Weld Metal Failure Data

In the analyses performed in Appendix A no distinction is made between the base metal and weld metal in the MPC shell. Procurement of the weld material, which is typically Type 308 stainless steel, and fabrication of the MPC in accordance with the requirements of the ASME Code ensures that the weld strength is equal to or greater than the base metal. However, it is generally known that weld-deposited

austenitic stainless steels (Type 308), although very ductile, have a tendency to be less ductile than the wrought (Type 304) product. At the high strain levels that may be encountered in beyond design basis events, such as severe drop impacts, this potential reduction in ductility of the deposited weld metal can be important to the structural integrity of the MPC shell.

In Reference B.18 twenty four Type 308 weld deposited metal specimens cut from fabricated weldments were statically tested at room temperature. The specimens were taken from both transverse and longitudinal orientations within the weldments. The mean value of the RA was 59.7% with a standard deviation of 9.1%. Using Equation (B.3), this converts to a mean true strain at failure of 0.91 in/in. The mean true strain at failure minus one and two standard deviations are 0.71 in/in and 0.54 in/in respectively.

In Reference B.19 the mechanical properties of archival Process Water System (primary coolant) piping and weld materials having approximately six years of service were measured. The Process Water System piping of the nuclear production reactors constructed in the 1950's at Savannah River Site was composed primarily of Type 304 stainless steel with Type 308 stainless steel weld filler. Tensile properties were measured for base metal, weld metal and heat-affected-zone (HAZ) materials. The test specimens represented both ASTM L-C and C-L orientations to allow comparison of the mechanical response for the cases of flaws oriented parallel and perpendicular to the pipe axis or rolling direction. The tensile properties of the archival piping material were found to be typical of recently produced commercial melts of Type 304 stainless steel piping. The values of the mean RA and standard deviation of the base metal, weld metal and HAZ material for static loading at room temperature are shown in Table B.1 below.

Table B.1: Reduction in Area Mean and Standard Deviation Test Results from Reference B.19.

Stainless Steel Material	Mean Reduction in Area (RA)	Standard Deviation
Type 304 Base Metal	72%	9.0%
Type 308 Weld Metal	61%	10.0%
Heat Effected Zone (HAZ)	71%	1.0%

The mean RA for the base metal of 72% in Table B.1 compares well to the typical values of 70% and 77% from References B.15 and B.16 respectively. Also, the mean RA for the weld metal of 61% and standard deviation of 10% compare well to the values of 59.7% and 9.1% cited in Reference B.18, discussed above. This data clearly shows that the 308 stainless steel weld metal is very ductile, although its ductility is slightly less than the ductility of the Type 304 base metal.

The reduction in area (RA) data for Type 308 stainless steel weld metal at room temperature and static loading used in the evaluation herein includes all of the data in References B.18 and B.19 discussed above, as well as dynamic test data at low strain rates (0.05/sec) from Reference B.19. Combining this data of 37 tests yields a mean RA of 59.0% and a standard deviation of 9.7%. These values establish the basis for determining the probability of weld failure and assumes that the weld failure data is normally distributed.

Temperature and Strain Rate Effects

In all the drop scenarios evaluated in Appendix A the most highly stressed region of the MPC occurs within the bottom foot of the shell (See Appendix A). While the MPC is being moved in the HI-TRAC

Transfer Cask, the temperature profile of the MPC shell, varies from 302 ºF at the bottom of the MPC to 445 ºF at the top (Reference B.1, Holtec HI-STORM FSAR Table 4.5.4). The test data used to calculate the mean RA and standard deviation, discussed above, is for static loading at room temperature. Typical RA values for Type 308 weld metal as a function of elevated temperature are reported in Figure 7 of Reference B.18. The trend curve in the figure shows that at 302 ºF, the temperature at the bottom of the MPC shell, the ratio of RA at room temperature to RA at temperature is 0.90. This factor is be used to adjust the RA room temperature values to those that would be expected at the higher temperature at the bottom of the MPC.

Strain rate can also have an effect on the ductility of stainless steel weldments. Typical strain rates for the drop impact scenarios considered in Appendix A are on the order of 100/sec. Reference B.20 shows that for strain rates of 1200/sec the ductility of stainless steel weldments deceases to about 88% of the static value. For a strain rate of 100/sec for Type 304 base metal, Reference B.15 shows that at 1000 ºF RA is approximately 7% greater than the value at room temperature. Based on the information in Reference B.20, a strain rate reduction factor of 0.98 was selected.

To account for both strain rate and temperature effects, the mean RA of 59.0% for weld metal was reduced by the factor 0.88 (0.90 x 0.98 = 0.88). This results in a mean RA of 52%, accounting for both strain rate and temperature. The standard deviation is assumed to remain the same at 9.7%. From Equation (B.3) the true strain at failure of stainless steel weld metal in a uniaxial tension test, considering the effects of strain rate and temperature, can be estimated to be 0.73 in/in with a mean minus one and two standard deviations of 0.55 in/in and 0.40 in/in respectively. Table B.2 below shows the mean true strain at failure minus several standard deviations along with the probability that the weld metal's true strain at failure is less than the tabulated value.

The probability of failure of stainless steel weld metal at the plastic strains given in Table B.2 are approximate, since the amount of test data capturing true strain at failure (or RA) of stainless steel weldments at elevated temperature and high strain rates is limited. Nevertheless, Table B.2 provides a reasonable estimate of weld failure probability in uniaxial tension at the strain rates and temperatures within the most highly stressed region of the MPC.

Table B.2: Mean true strain at failure minus several standard deviations, and the probability that the weld metal's true strain at failure is less than the tabulated value.

Standard Deviation from the Mean	True Strain at Failure (TSF) (in/in)	Probability the TSF is Less than the Tabulated Value [x < TSF]
0.0 (Mean)	0.73	0.5000
0.5	0.64	0.3085
1.0	0.55	0.1587
1.5	0.47	0.0668
2.0	0.40	0.0228
2.5	0.32	0.0062
3.0	0.26	0.0013
3.5	0.20	0.00023
4.0	0.14	0.000032
4.5	0.087	0.000003
5.0	0.036	< 0.000001

Effect of State of Stress

For each drop scenario, the maximum effective plastic strain in the MPC shell was calculated in Appendix A. However, cracking of a stainless steel weldment cannot be determined by simply comparing the calculated maximum effective plastic strain to the true strain at failure even when temperature and strain rate have been considered. This is due to the fact that the effective plastic strain was calculated from a complex three dimensional state of stress, while the true strain at failure was derived from a one dimensional state of stress. Unlike a one dimensional state of stress, a three dimensional state of stress may constrain plastic flow in the material and lower the effective plastic strain at which failure occurs. This loss of ductility can be accounted for by the use of a Triaxiality Factor (TF), which is the ratio of normal stress to shear stress on the octahedral plane, normalized to unity for simple tension, as given by Equation (B.4) (References B.21 and B.22).

$$Triaxiality\ Factor = \frac{\sigma_1 + \sigma_2 + \sigma_3}{\frac{1}{\sqrt{2}}\left[\left(\sigma_1 - \sigma_2\right)^2 + \left(\sigma_2 - \sigma_3\right)^2 + \left(\sigma_3 - \sigma_1\right)^2\right]^{1/2}} \qquad \text{(B.4)}$$

where, σ_1 = maximum principal stress,
σ_2 = intermediate principal stress, and
σ_3 = minimum principal stress.

The reduction in ductility associated with the triaxial stress state is approximately equal to the true strain at failure in uniaxial tension divided by the Triaxiality Factor. More precisely, the ratio of effective plastic strain (EPS) at failure to the true strain at failure in uniaxial tension, which is called the ductility ratio (DR), is given by Equation (B.5) (Reference B.23).

$$DR = 2^{(1 - TF)} \tag{B.5}$$

where, DR = The Ductility Ratio, and
TF = The Triaxiality Factor

Thus, to determine the actual strain at which weld cracking will initiate requires that either the calculated effective plastic strain or the true strain at failure be adjusted to account for the triaxial nature of the state of stress. [Note that TF = 1.0 represents uniaxial tension. TFs greater than 1.0 are produced by states of stress that constrain plastic flow, reduce ductility and result in a higher likelihood of failure for a given EPS. TFs less than 1.0 are produced by states of stress that enhance plastic flow, increase ductility and result in a lower likelihood of failure for a given EPS.]

Probability of Weld Failure

The probability that the true strain at which a weld fails is less than the calculated maximum effective plastic strain (EPS) cannot be determined directly from Table B.2. To use Table B.2 to determine the probability of weld failure, the calculated maximum effective plastic strain must first be divided by the ductility ratio (DR) to adjust it for the effects of the triaxial stress state at the location where the EPS occurs. However, the location (element) where the maximum EPS occurs may not be the location most susceptible to failure. The location where the probability of failure is greatest is where the quotient of EPS divided by the DR results in the highest value. For example, in the case of the 100 foot drop of the Transfer Cask onto the concrete floor a maximum EPS of 0.256 in/in occurred in element 15997 on the inside surface of the MPC shell beneath the basket support, as shown in Figure A.13 . For this element the triaxiality factor (TF) is negative, indicating a very favorable state of stress, and the EPS adjusted for triaxiality is 0.13 in/in. For this lower EPS the probability of failure decreases considerably. Thus the element with the calculated maximum EPS does not necessarily control failure.

To determine the location where the maximum EPS adjusted for triaxiality occurs, a set of elements with high values of EPS and attributes likely to result in a high TF were selected for evaluation. For these elements, EPS, TF, DR and adjusted EPS were calculated at each output time. This was done for the 100, 70 and 40 foot drops of the transfer cask onto the concrete floor and for the 19 foot drop of the MPC into the storage overpack. For the 5 foot drop of the transfer cask onto the concrete floor and for drops of the transfer cask onto the storage overpack, the maximum EPS together with the maximum TF for a biaxial stress state of 2.0 were used to conservatively calculate the maximum EPS adjusted for triaxiality.

Transfer Cask and MPC Drop Events

For drops of the Transfer Cask falling onto the concrete floor, Table B.3 gives the calculated maximum effective plastic strain (EPS), the maximum EPS adjusted for triaxiality, and the probability of weld crack initiation. It is important to emphasize that the probability of weld crack initiation is calculated using the maximum EPS adjusted for triaxiality when using Table B.2. Table B.4 provides the same information

for the drop of the Transfer Cask onto the Storage Overpack, and Table B.5 shows the results for the 19 foot drop of the MPC into the Storage Overpack.

Table B.3: Probability of MPC Weld Crack Initiation from the Drop of the Transfer Cask onto the Concrete Floor

Drop Height (feet)	Maximum Effective Plastic Strain (EPS) (in/in)	Maximum Effective Plastic Strain Adjusted for Triaxiality (in/in)	Probability of Weld Crack Initiation (1)
5	0.024	0.048 (2)	< 0.000001
40	0.195	0.213	0.000360
70	0.240	0.285	0.002600
100	0.256	0.385	0.019600

(1) The term "weld crack initiation" or "cracking of the MPC weld" is used in place of "weld failure" or "failure of the MPC weld" to distinguish between a "crack" in the weld, that may not propagate through the entire thickness, and "failure" of the weld, which would imply a through thickness rupture of the weld and breach of the confinement boundary. When developing a weld failure criterion using uniaxial tension tests the terms failure, rupture and breach are synonymous. However, when the maximum EPS occurs on the surface of a region of high bending curvature, the initiation of a failure -- a crack – does not necessarily result in a rupture or breach. Thus, some caution is required when using the word "failure" to describe what happens when a failure limit is reached at a point on the surface of a region with high curvature (strain gradient), especially when the energy input is limited.

(2) A maximum Triaxiality Factor of 2.0 was used.

Table B.4: Probability of Weld Crack Initiation for the Drop of the Transfer Cask onto the StorageOverpack

Drop Height (feet)	Maximum Effective Plastic Strain at Element 9421 (1) (in/in)	Maximum Effective Plastic Strain Adjusted for Triaxiality (2) (in/in)	Probability of Weld Crack Initiation
5	0.0363	0.0726	0.000002
40	0.0601	0.1202	0.000014
80	0.0976	0.1952	0.000203

(1) See Table A.4 note 2.

(2) A maximum Triaxiality Factor of 2.0 was used.

Table B.5: Probability of Weld Crack Initiation for the 19 foot Drop of the MPC into the Storage Overpack

Drop Height (feet)	Maximum Effective Plastic Strain (in/in)	Maximum Effective Plastic Strain Adjusted for Triaxiality (in/in)	Probability of Weld Crack Initiation (1)
19	0.456	0.623	0.282

(1) See Note 1 from Table B.3 and discussion below related to tearing of the basket support fillet welds for the 19 foot drop.

The 19 foot drop of the MPC into the storage overpack results in the highest probability (0.282) that a weld on the MPC confinement boundary will crack on impact. This result, as well as the results for the other drop events, must be viewed as a very conservative estimate of the probability of MPC confinement boundary breach or rupture. There are two reasons for this:

(1) The probability of weld crack initiation is the probability that the most highly stressed element of the six elements through the thickness of the MPC shell will fail. Because this occurs in a region of high curvature in a highly indeterminate structure, the failure of one element on the surface of the shell will result in the redistribution of internal forces to the stiffer (in bending) adjacent elements on the surface, with little of the internal forces redistributing to the lower stressed interior elements through the thickness. This makes it more likely that additional surface elements will fail, and less likely for the failure to propagate through the thickness. In addition, the process itself is contained, since the total kinetic energy is limited, as in all impact events.

(2) The maximum EPS of 0.456 in/in and the adjusted maximum EPS of 0.623 in/in result from constraint imposed on the MPC shell. This constraint is created by the discontinuous basket support "stiffeners" that terminate 1.5 inches above the MPC base plate. The constraint on the shell imposed by the support is maintained by the 1" long 1/8" fillet weld that attaches the bottom portion of the support to the shell. Figure B.3 shows the deformation and contours of EPS in this region, and Figure B.4 shows the shear deformation and the very evident shear-lag in the elements of the support at the location of the fillet weld between nodes 18469 and 21444 . (This basket support is the same one shown in Figure A.26.) In the likely event this weld tears during impact, the local constraint on the shell is relieved and the shell will behave locally as though it were unstiffened. A published analysis (Reference B.24) of a 25'drop of the MPC onto a rigid surface, in which the basket supports were not included, produced a maximum EPS of 0.21 in/ in, which is a significant reduction from the value of 0.456 in/in when the attachment welds remain intact. Thus, the potential tearing of these small attachment welds can significantly reduce the probability that a weld on the confinement boundary may crack.

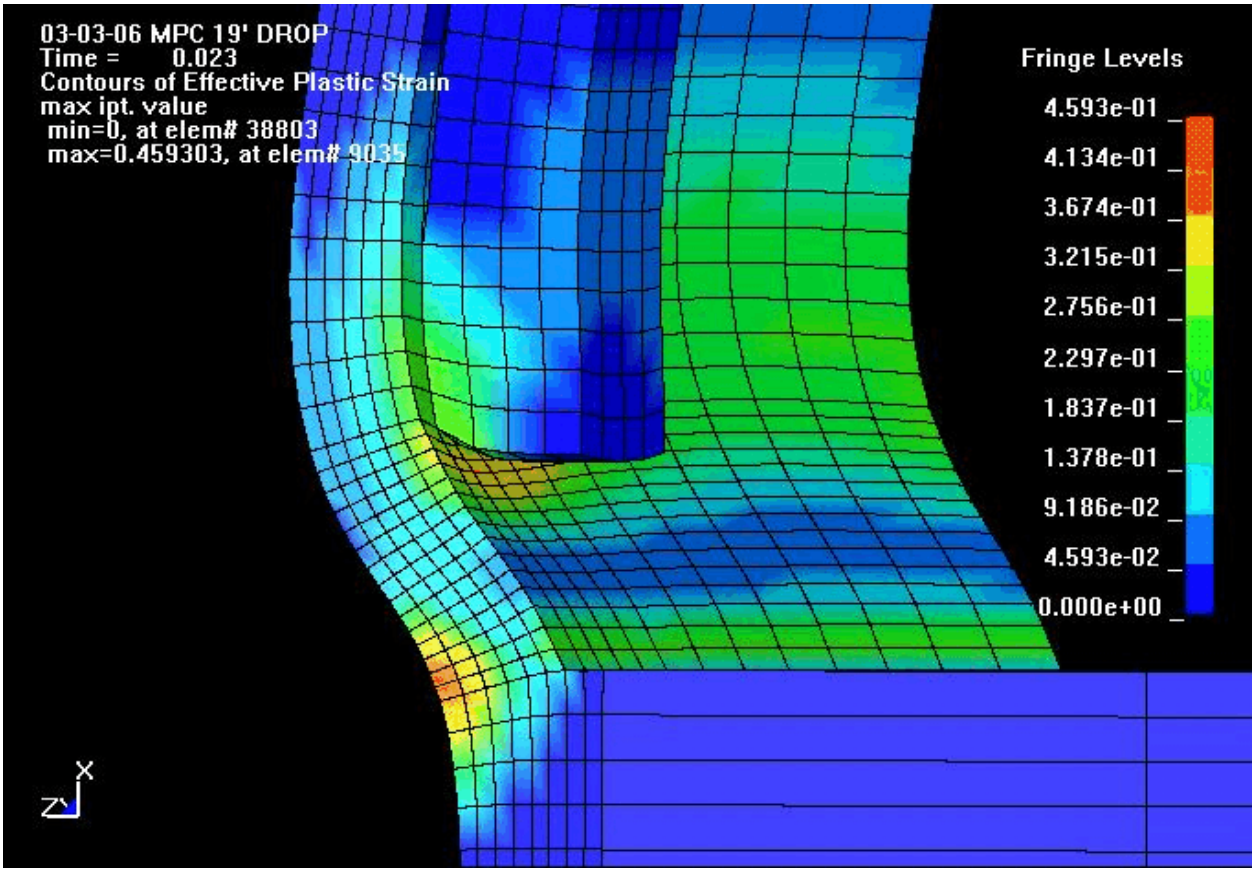

Figure B.3. Deformation and contours of EPS in the vicinity of the stitch weld attaching the basket support to the shell.

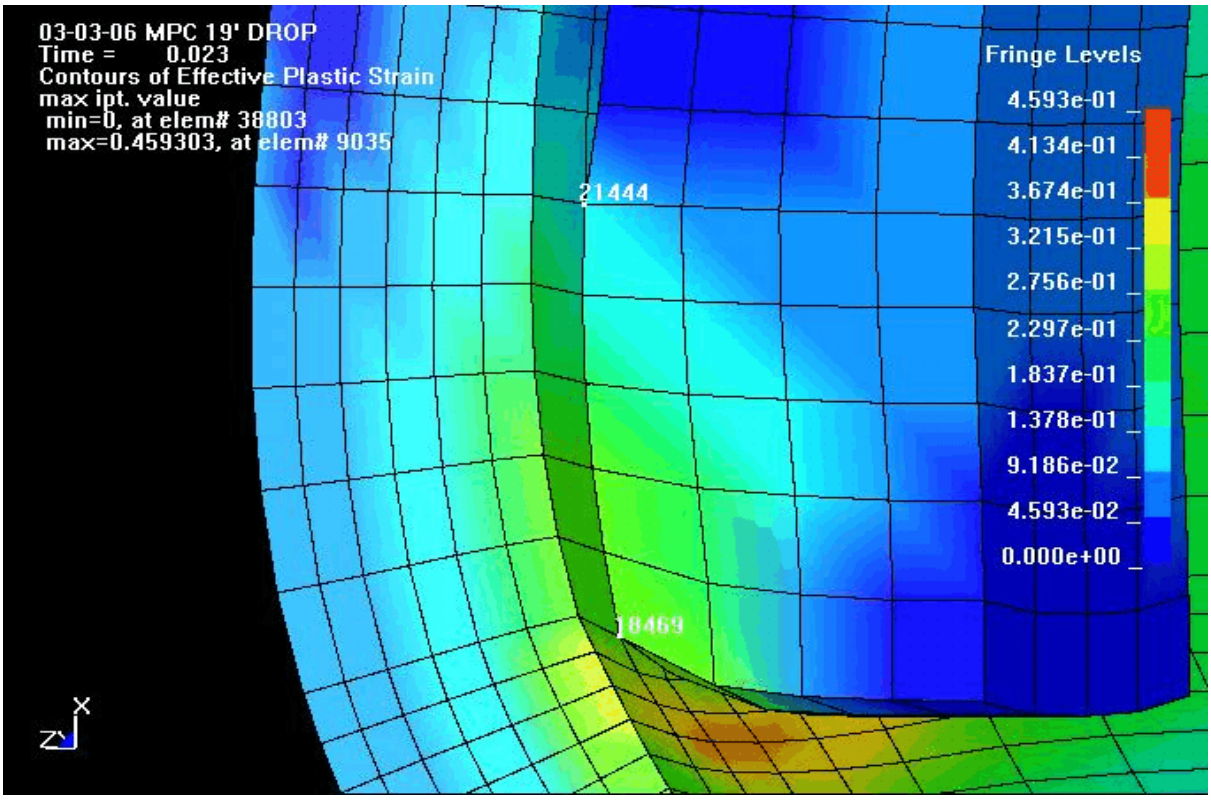

Figure B.4. Shear deformation and shear-lag are evident in the elements of the support at the location of the fillet weld between nodes 18469 and 21444 .

Storage Cask Tip-Over Event

The storage cask tip-over event is discussed in Section A.4.6. The maximum stresses in the MPC for this event are given in Table A.6 and come from the HI-STORM 100 Safety Analysis Report (Reference B.1). The maximum stress (stress intensity) is approximately 59,000 psi, which is less than the allowable stress intensity for primary membrane plus bending of 65,200 psi for this Service Level. For the purpose of evaluating weld fracture, the allowable stress of 65,200 psi is used herein. In accordance with the ASME B&PV Code the maximum stress would have been calculated from a linear-elastic analysis, and in this case the analysis produced stresses that exceed the yield stress of 38,000 psi at temperature (Table A.2). Therefore, the maximum stress of 65,200 psi cannot be converted to a strain simply by dividing by the elastic modulus.

Since the weld failure criterion is based on plastic strain, the elastically calculated maximum stress must be converted to a plastic strain that could have reasonably resulted from a non-linear analysis of the same event. Also, since the "damage" that can be inflicted on the MPC during a tip-over event is energy limited, an energy balance approach can be used to estimate the maximum plastic strain. In this approach the strain energy per unit volume absorbed at the point of the elastically calculated maximum stress is equated to the strain energy per unit volume absorbed through elastic-plastic deformation of the material using the idealized engineering stress-strain curve in the LS-DYNA program that was used for the drop analyses.

Using this approach and the data in Table A.2, the calculated maximum plastic strain is 0.0031 in/in. Since the maximum membrane plus bending stress must have occurred on the boundary, the maximum value that the triaxiality factor can be is 2.0. The maximum adjusted plastic strain is therefore 0.0062 in/in. Assuming that the maximum plastic strain occurs at one of the axial or circumferential welds, the probability of weld crack initiation from Table B.2 is less than 0.000001. This result is summarized in Table B.6 below.

Table B.6: Probability of Weld Crack Initiation from Storage Cask Tip-over

	Estimated Maximum Plastic Strain (in/in)	Maximum Plastic Strain Adjusted for Triaxiality (in/in)	Probability of Weld Crack Initiation (1)
Storage Cask Tip-over Event	0.0031	0.0062	< 0.000001

(1) See Note 1 from Table B.3.

B.1.5 Failure Analysis Inputs for Limit Load and Creep Rupture

In order to determine the probability of MPC failure for the limit load and creep rupture, distributions of the following material properties are needed at various temperatures:

1. Yield strength,
2. Tensile strength, and
3. Creep rupture strength.

In addition to the material properties, stress concentration factors are also needed.

The MPC may be constructed from several different types of austenitic stainless steels. In general, the tensile and creep rupture properties of Type 304 stainless steel tend to be more limiting regarding MPC failure than other types of austenitic steels. Therefore, yield, tensile and creep rupture strengths used in the failure analyses are based on Type 304 stainless steel. Comparisons between the material properties of Type 304 and 316 are given in the sections that follow.

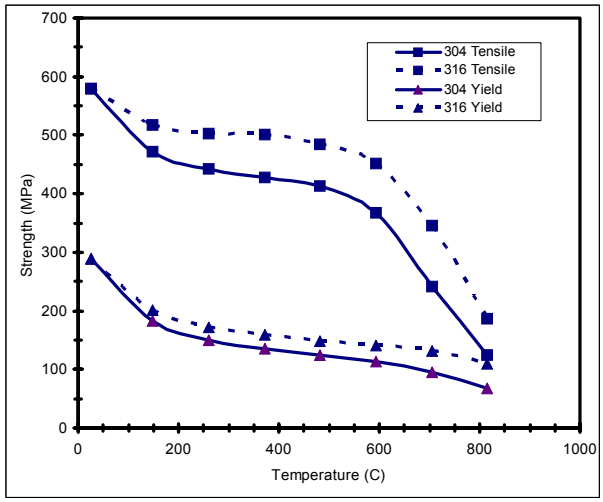

Figure B.5: Yield and Tensile Strength Behavior of Type 304 and 316 Austenitic Stainless Steels at Elevated Temperatures (References B.2-B.3)

Yield and Tensile Strength

The yield and tensile strength of austenitic stainless steel decreases as the material temperature increases. Figure B.5 compares representative yield and tensile strengths for Type 304 and 316 stainless steel over a wide range of temperatures (References B.2 and B.3). Even though the *required* minimum room temperature yield and tensile strengths for these two

materials are identical, this figure shows that *typically* Type 316 has higher yield and tensile strengths between 24°C (75°F) and 816°C (1500°F). Therefore, the tensile properties used in the failure analysis of the MPC are for Type 304 stainless steel.

Table B.7 describes the reduction in yield and tensile strength of Type 304 stainless steel with temperature as a fraction of the yield and tensile strength at room temperature (Reference B.3). This same reference cites mean room temperature yield and tensile strengths for this material as 254 MPa (36,900 psi) and 578 MPa (83,900 psi), respectively. The standard deviations are 44 MPa (6,400 psi) for yield strength and 30 MPa (4,300 psi) for tensile strength.

Table B.7: Reduction in Yield and Tensile Strengths of Type 304 Stainless Steel as a Function of Temperature

Temperature °C (°F)	Yield Strength Reduction Ratio	Best Estimate Yield Strength[1] Mpa (psi)	Minimum Yield Strength[2] Mpa (psi)	Tensile Strength Reduction Ratio	Best Estimate Tensile Strength[3] Mpa (psi)	Minimum Tensile Strength[4] Mpa (psi)
24 (75)	1.00	254 (36900)	207 (30000)	1.00	578 (83900)	517 (75000)
38 (100)	0.96	244 (35424)	207 (30000)	0.97	561 (81383)	517 (75000)
93 (200)	0.83	211 (30627)	172 (25000)	0.86	497 (72154)	490 (71000)
149 (300)	0.75	191 (27675)	155 (22500)	0.80	463 (67120)	455 (66000)
204 (400)	0.69	176 (25461)	143 (20700)	0.78	451 (65442)	444 (64400)
260 (500)	0.65	165 (23985)	134 (19400)	0.77	445 (64603)	438 (63500)
316 (600)	0.61	155 (22509)	125 (18200)	0.77	445 (64603)	435 (63100)
371 (700)	0.59	150 (21771)	119 (17300)	0.77	445 (64603)	431 (62500)
427 (800)	0.56	142 (20664)	114 (16600)	0.76	440 (63764)	425 (61700)
482 (900)	0.54	137 (19926)	112 (16200)	0.74	428 (62086)	383 (55500)
538 (1000)	0.52	132 (19188)	108 (15600)	0.70	405 (58730)	362 (52500)
593 (1100)	0.49	125 (18081)	101 (14700)	0.63	364 (52857)	326 (47250)
649 (1200)	0.47	120 (17343)	97 (14100)	0.55	318 (46145)	284 (41250)
704 (1300)	0.44	112 (16236)	91 (13200)	0.46	266 (38594)	238 (34500)
760 (1400)	0.39	99 (14391)	81 (11700)	0.35	202 (29365)	181 (26250)
816 (1500)	0.31	79 (11439)	64 (9300)	0.25	145 (20975)	129 (18750)
871 (1600)	0.20	51 (7380)	41 (6000)			

Notes:

1. Best estimate yield strengths based on reduction ratios and room temperature yield strength of 36,900 psi (Reference B.3).
2. Minimum yield strengths from 75 °F to 800 °F taken from ASME Code. Minimum yield strengths from 900 °F to 1600 °F calculated using reduction ratios and ASME minimum at 75 °F.
3. Best estimate tensile strengths based on reduction ratios and room temperature tensile strength of 83,900 psi (Reference B.3).
4. Minimum tensile strengths from 75 °F to 800 °F taken from ASME Code. Minimum tensile strengths from 900 °F to 1600 °F calculated using reduction ratios and ASME minimum at 75 °F.

Best estimate yield and tensile strengths at various temperatures were determined using these reduction ratios and room temperature properties. Table B.7 lists these best estimate values at temperatures up to 871°C (1600°F).

The American Society of Mechanical Engineers (ASME) code places minimum allowable yield and tensile strengths for this material at temperatures up to 427°C (800°F). These minimums are also shown in Table B.7. At temperatures above 427°C (800°F), the minimum allowable yield and tensile strengths were determined by applying the reduction ratios to the ASME minimums at room temperature.

Figure B.6 shows the decrease in the best estimate and minimum tensile properties of Type 304 stainless steel at increased temperatures. The minimum allowable tensile strengths are very close to the best estimate values. Above 427°C (800°F) this difference increases. For the yield strengths, the difference between the minimum and best estimate values slowly decrease at higher temperatures.

It was assumed that both the yield and tensile properties of Type 304 stainless steel at any given temperature could be described by a normal distribution with a mean equal to the best estimate value at that temperature. In addition the standard deviations defined above were assumed to apply at all temperatures. Tensile properties at temperature between those listed in Table B.7 were calculated by interpolation.

Type 304 stainless steel base metals are typically welded using Type 308 as the weld filler metal. The minimum required room temperature yield strengths and tensile strengths are identical for both of these materials. Table B.8 lists some elevated temperature tensile properties for Type 308 austenitic stainless steel.

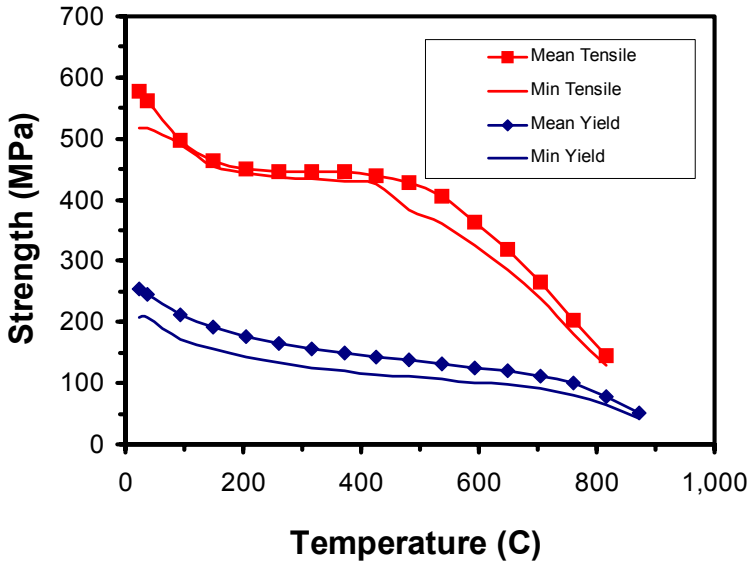

Figure B.6: Yield and Tensile Strength Behavior of Type 304 Austenitic Stainless Steels at Elevated Temperatures (Reference B.3)

Table B.8. Tensile Properties for Type 308 Stainless Steel at Elevated Temperatures

Temperature °C (°F)	Yield Strength Mpa (Psi)	Tensile Strength Mpa (Psi)
482 (900)	310 (45,000)	444 (64,400)
593 (1100)	261 (37,800)	301 (43,700)
649 (1200)	222 (32,200)	239 (34,700)

Comparing Tables B.7 and B.8 shows that the expected weld material (Type 308) is expected to have superior tensile properties to that of the base metal (Type 304). Therefore, the properties listed in Table B.1 can conservatively be used to describe the MPC welds and plates.

Creep Rupture Strength

Creep rupture strength of Type 304 stainless steel was compiled from data in the open literature (References B.2 to B.7). It should be noted that this creep rupture data is not comprehensive. The time and temperature conditions for this data were converted to the Larson-Miller parameter (Reference B.17).

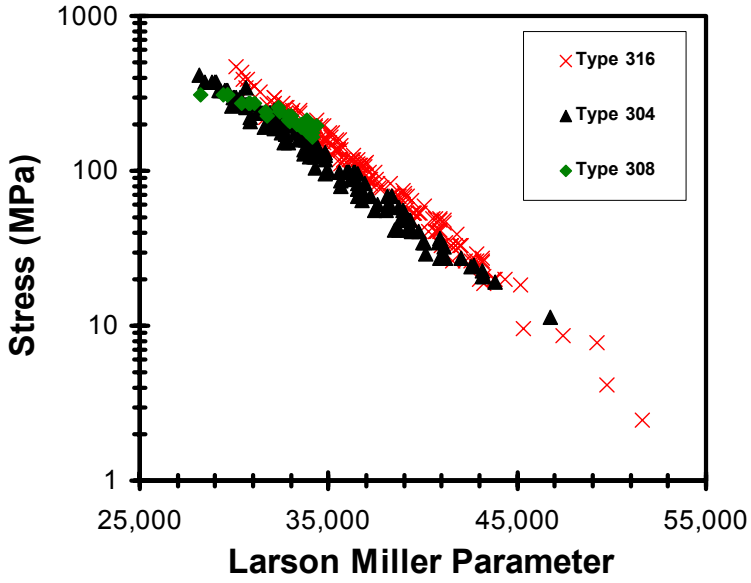

Figure B.7: Creep Rupture Properties of Type 304, 308, and 316 Austenitic Stainless Steels (References B.2 - B.7)

$$LarsonMiller \equiv T \bullet (C + \log(t_r)) \qquad \text{(B.6)}$$

where: T = Temperature in °R (= ^{o}F + 459.67)
C = constant (18 for austenitic stainless steel)
t_r = time to rupture in hours.

Figure B.7 shows the stress at creep rupture data plotted as a function of this Larson-Miller parameter for Types 304, 316, and 308 austenitic stainless steels. For a given Larson-Miller parameter value, Type 316 tends to have a higher creep rupture stress. The data for Type 304 and 308 are similar. Therefore, the creep rupture data used for the MPC failure analysis is based upon Type 304 material properties. This data is used to model both the plate and weld material properties.

Figure B.8 is typically how creep rupture data is presented. However, for the purposes of developing a creep rupture model, the Larson-Miller parameter is needed as a function of the applied stress. Figure B.7 shows the Larson-Miller parameter plotted as a function of the log of applied stress for only Type 304

materials. The data was fit to a line with an R^2 value of 0.98. The equation of this line has a slope of –11,032 and a y-intercept of 81,404. The best fit, 95% upper bound, and 95% lower bound trend lines are also shown in Figure B.8.

At a given stress, there is some variability in the Larson-Miller parameter required to cause creep rupture of Type 304 stainless steel. It is assumed that this variability in Larson-Miller parameter is normally distributed about a mean value given by the best-fit line described above. It is also assumed that the 95% bounds represent 2 standard deviations about this mean value. Therefore, both the mean and standard deviation of the Larson-Miller parameter vary with the applied stress.

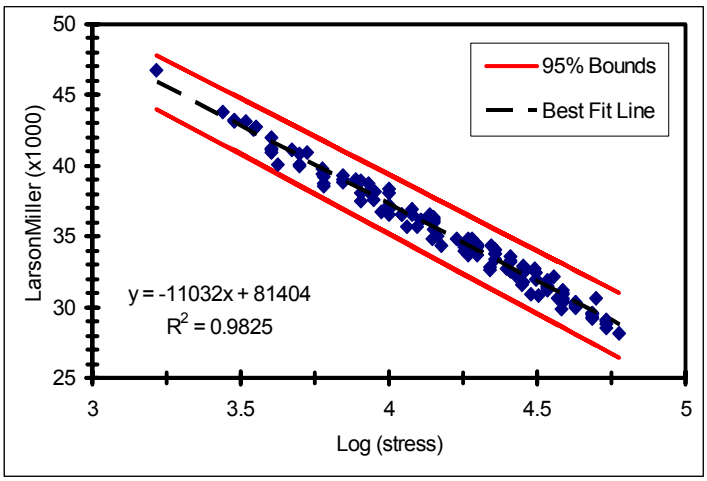

Figure B.8: Best Estimate and Bounding Larson-Miller Parameters as a Function of Log (Stress) for Type 304 Austenitic Stainless Steel

Flaw Distribution

An analysis of the MPC welds was performed using the PRODIGAL computer code to obtain flaw distributions for the failure analyses. The PRODIGAL code is described in several of the references listed at the end of this report (References B.8 - B.11). These references also describe a number of applications of the code to nuclear pressure vessels and piping. Other references describe studies that have collected data on observed flaws in welded construction and have compared the numbers and sizes of the observed flaws with predictions made with the PRODIGAL code (References B.12 and B.13).

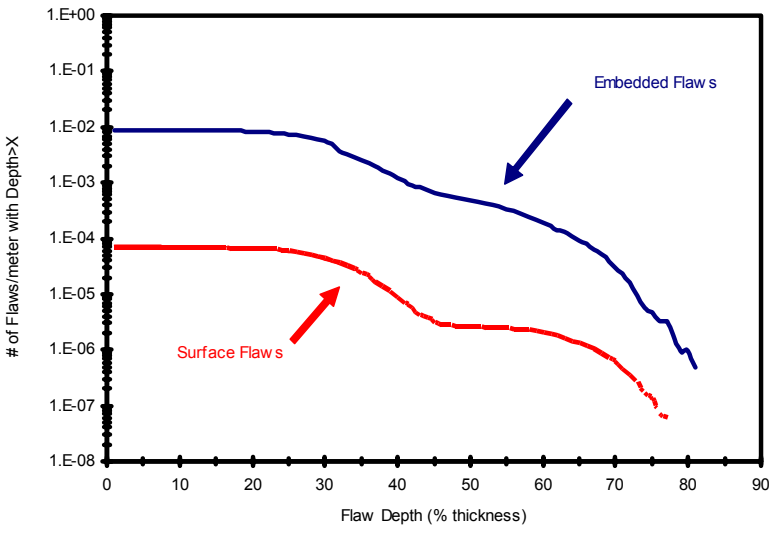

Figure B.9: Prodigal Flaw Distribution Results for MPC Welds. Total Number of Flaws with Depth Greater than a Given Depth

The PRODIGAL code is an expert system model that simulates the occurrence of flaws in nuclear grade welding. An additional aspect of the model is the simulation of the radiography and dye-penetrant inspections performed to detect flaws so that defective welds can be rejected and/or repaired. The focus of PRODIGAL is on crack-like flaws that have the potential to impact structural integrity. Specific limitations of the model are that it excludes structurally benign flaws such as pores and rounded slag. The model does not address certain inspections such as ultrasonic examinations (UT) and leak testing. It was designed to predict the expected defect distributions in an average weld but does not include a consideration of uncertainties or the expected weld-to-weld variations.

PRODIGAL outputs the size, number, and location of flaws per meter of weld. The total number of flaws per meter of weld with a depth greater than a given percentage of weld thickness is shown in Figure B.9. This figure also distinguishes between surface breaking and embedded flaws in the weld. The results show that MPC welds have more embedded flaws than surface breaking flaws. The largest flaw predicted by PRODIGAL is approximately 80% of the weld thickness.

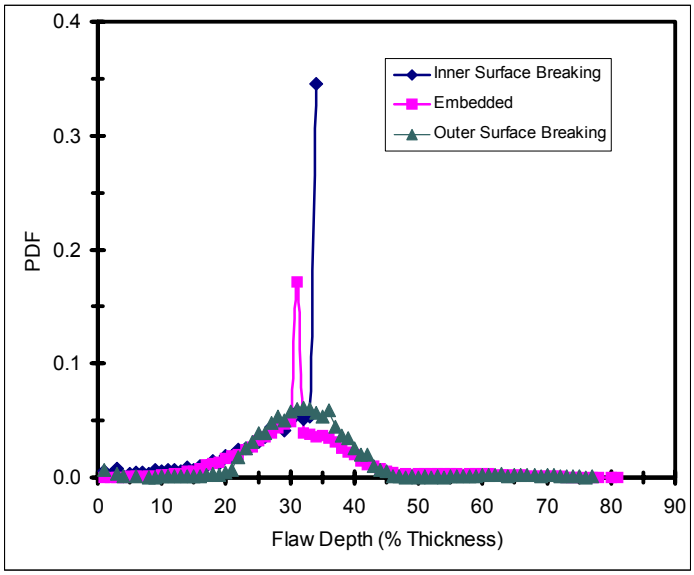

Figure B.10: Probability Distributions of Flaw Depths for MPC Welds Based on PRODIGAL Results

There are 6 shell welds in each MPC. This includes 4 axial welds, 1 circumferential weld, and 1 shell-to-baseplate weld. The length of 2 axial welds on each side of the MPC is 4.77 m (15.65 ft). These 2 axial welds are modeled as 1 continuous weld extending the entire height of the MPC. The length of the circumferential and shell-to-baseplate weld is 5.46 m (17.9 ft) each. The total number of flaws in each of the MPC welds can be calculated by taking the PRODIGAL results and multiplying by these weld lengths. There are approximately 0.04 flaws per axial weld extending the entire height of the MPC. The circumferential and shell-to-baseplate welds each have approximately 0.05 flaws per weld. In other words, 1 in 25 (0.04) axial welds will contain a flaw while 1 in 20 (0.05) circumferential or shell to baseplate welds are expected to contain a fabrication flaw.

If a flaw is present in an MPC weld, the location of the flaw is also based on PRODIGAL results. The flaws in the MPC welds were separated into three locations, inner surface breaking, outer surface breaking, and embedded. Analysis of PRODIGAL results showed that 98.44% of the flaws were expected to be embedded, 0.83% were inner surface breaking, and 0.73% were expected to be outer surface breaking.

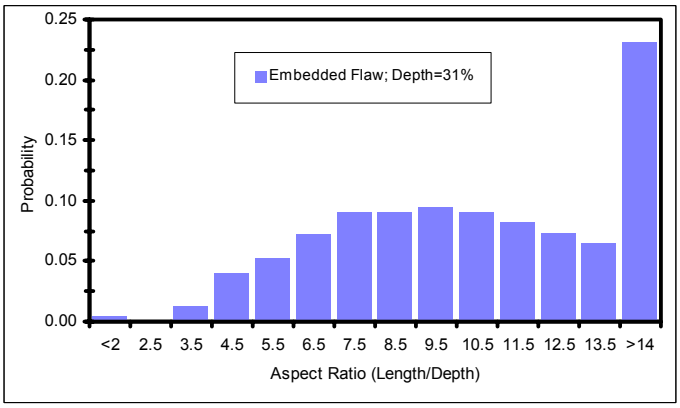

Figure B.11: Distribution of Aspect Ratios for an Embedded Flaw with a Depth of 31% of the Weld Thickness

Given a flaw in a particular location, a probability distribution of flaw depths was determined as follows. In the PRODIGAL analysis, 1,000,000 meters of weld were simulated. The PRODIGAL output for a given flaw depth was multiplied by 1,000,000 meters to give the number of simulated flaws of that flaw depth. Summing these values for all flaw depths gives the total number of simulated flaws. The probability of obtaining a flaw of a given depth was calculated by dividing the number of simulated flaws of that depth by the total number of simulated flaws. This process was performed for inner surface breaking flaws, outer surface breaking flaws, and embedded flaws. The resulting probability distributions are shown in Figure B.10. The most likely flaw depth present in these welds is approximately ⅓ of the wall thickness. This is expected, since the flaw depths predicted by PRODIGAL are a function of the size of the welding bead and the welds are fabricated in 3 passes.

For a given flaw location and depth, PRODIGAL also provides a range of flaw aspect ratios (flaw length/flaw depth). PRODIGAL reports these aspect ratios in 14 bins ranging from less than 2 to greater than 14. A probability distribution of aspect ratios was determined for each flaw depth and location based on these results. An example of the aspect ratio probability distribution is shown in Figure B.11 for an embedded flaw with a depth of 31% of the weld thickness. The probability of the last bin (>14) is much larger than the other bins in this histogram because this bins includes the entire tail of the distribution representing all flaws with an aspect ratio greater than 14.

Stress Concentration

A stress concentration is present at the shell-to-baseplate weld because of the discontinuity formed where the MPC shell and baseplate connect. The maximum stress concentration occurs at the surface and quickly approaches a value of 1 away from the shell surface. The equation used to estimate this stress concentration is given below:

$$C = \left[1 + 0.5\left(\frac{r}{r+x}\right)^2 + 2.5\left(\frac{r}{r+x}\right)^4 \right] \tag{B.7}$$

where: C = bending stress concentration in shell to baseplate weld
r = fillet radius (taken as 0.01 inches or 0.0254 cm)
x = depth from shell surface

This equation is based on the stress distribution for a circular hole of radius, r, in a plate under tension, where the maximum stress concentration factor has been increased to 4 in order to be more representative of a small radius fillet.

For the shell-to-baseplate weld, the bending stress at a given thickness location was determined by multiplying the nominal bending stress by this stress concentration.

B.1.6 Limit Load Model

A flow stress model was also used to predict MPC failure. Failure occurs if the applied membrane stress due to internal pressure equals or exceeds the flow stress of the material.

$$\sigma_{flow}^{membrane} \equiv \frac{(\sigma_{yld} + \sigma_{uts})}{2} \tag{B.8}$$

where : σ_{flow} = flow stress
σ_{yld} = yield strength
σ_{uts} = tensile strength

The Level D stress limits in this material for membrane plus primary bending as specified in Section III of the ASME Code is 150% of the primary membrane limit. Using the above definition for flow stress as the primary membrane limit, the membrane plus bending stress limit is given below:

$$\sigma_{flow}^{membrane+bending} \equiv 0.75 \bullet (\sigma_{yld} + \sigma_{uts}) \tag{B.9}$$

At a given temperature, the applied stresses were calculated using the equations in Section B.1.2. The yield and ultimate tensile strengths of the material were sampled so the critical flow stress values could be

determined. If the circumferential or axial stresses of the MPC were greater than the membrane flow stress, failure was predicted. Similarly, if the bending and membrane stress of the MPC shell to baseplate exceeded the membrane plus bending flow stress, failure was also predicted. If either of these limits were exceeded, the entire MPC was considered failed.

Again, the probability of failure due to exceeding critical flow stress was calculated by performing Monte Carlo simulations at various temperatures. The probability of MPC failure was defined as the number of MPC failures divided by the total number of iterations.

The sampled values were correlated such that if a mean plus 1 standard deviation value of yield stress was sampled then a mean plus 1 standard deviation tensile strength was sampled. The yield and tensile strengths sampled in this model were allowed to fall below the minimum values defined in Table B.1. Even with the yield and tensile strengths below the minimum allowables, the limit load model never contributed to failure for any of the heat-up scenarios.

B.1.7 Creep Rupture Model

The methodology used to predict creep rupture of the MPC is based on the model developed by Argonne National Laboratory for creep rupture of steam generator tubes (Reference B.14). In this model, the structure accumulates a fraction of creep damage after exposure to any specific time/temperature/stress condition. If the sum of these creep damage fractions exceeds one, failure is predicted. In equation form this failure criteria becomes

$$\int_0^{t_f} \frac{dt}{t_r(T,\, m_p \cdot \sigma)} \equiv 1 \qquad \text{(B.10)}$$

where: $t_r(T,\sigma)$ = time to cause rupture at temperature, T, and stress, σ
dt = time spent at temperature, T, and stress, σ
t_f = total time

The above description applies to unflawed structures. If cracks are present, then the above failure criteria is modified by multiplying the stress in an unflawed structure by an appropriate magnification factor, m_p.

$$\int_0^{t_f} \frac{dt}{t_r(T,\sigma)} \equiv 1 \qquad \text{(B.11)}$$

The stress magnification factors for part through axial and circumferential flaws are given below. For axial flaws, the magnification factors are given by Equations B.12

$$m_p \equiv \frac{1-\alpha \bullet \frac{a}{m \bullet t}}{1-\frac{a}{t}} \qquad \text{(B.12a)}$$

$$\alpha \equiv 1 + 0.9 \bullet \left(\frac{a}{t}\right)^2 \bullet \left(1 - \frac{1}{m}\right) \tag{B.12b}$$

$$m \equiv 0.614 + 0.481 \bullet \lambda + 0.386 \bullet \exp(-1.25 \bullet \lambda) \tag{B.12c}$$

$$\lambda \equiv \frac{1.82 \bullet c}{\sqrt{r_{mean} \bullet t}} \tag{B.12d}$$

where: m_p = magnification factor
a = flaw depth
c = flaw length
t = MPC shell thickness (= 0.5 in or 1.27 cm)
r_{mean} = mean radius of MPC (= 33.9375 in or 86.2 cm)

For circumferential flaws, the magnification factors are given by Equations B.13.

$$m_p \equiv \frac{1}{\left[m + \left(\frac{\theta}{\pi}\right) \bullet \left(1 - \frac{a}{t} - m\right)\right]} \tag{B.13a}$$

$$m \equiv \frac{1 - \frac{a}{t}}{1 - \frac{a}{N \bullet t}} \tag{B.13b}$$

$$N \equiv 1 + 0.2 \bullet \left(\frac{\theta}{\pi}\right)^{0.2} \tag{B.13c}$$

where: a = flaw depth
θ = one half angular length of flaw
t = MPC shell thickness = 0.5 in (1.27 cm)

The probability of creep rupture failure as a function of temperature was determined as follows. The MPC stresses at any time-temperature condition were determined using the equations in Section B.1.2. For this stress, the Larson-Miller parameter required to cause creep rupture was sampled from the distribution described in Section B.1.5. Given this temperature and Larson-Miller parameter, the time required to cause creep rupture failure, $t_r(T,\sigma)$, can be determined. The incremental creep damage is calculated by dividing the actual time spent in these conditions, dt, by the time needed to cause creep rupture, $t_r(T,\sigma)$. This procedure is repeated for the next time-temperature-stress condition. If at the temperature of interest, the summation of creep damage fractions is greater than one, MPC failure is predicted.

Over time the heat load in the cask would slowly drop. This heat reduction would cause a corresponding reduction in MPC temperature and internal pressure. This effect was not modeled in the thermal analyses; so it was assumed that the internal heat load remained constant for the entire 20 year license period of the cask.

Monte-Carlo simulations were performed on MPCs to determine the probability of creep rupture failure. A simulated MPC consisted of both flawed and unflawed regions. The flawed regions consisted of the axial welds, one circumferential weld and one shell to baseplate weld. The unflawed regions were made up of the MPC shell plates. The creep rupture analysis assumed that all flaws were located on the weld surface. If any of the regions were predicted to fail, the entire MPC was counted as a failure. The probability of MPC failure is the number of failures divided by the number of simulations performed.

B.1.8 Results

Mechanical loads

Table B.9 shows the probability of the failure of a single finite element (i.e., the probability of weld crack initiation) through the thickness of the MPC shell for (1) the drop of the Transfer Cask onto the concrete floor from 100, 70, 40 and 5 feet, (2) the drop of the Transfer Cask onto the Storage Overpack from 80, 40 and 5 feet, (3) the drop of the MPC into the Storage Overpack from 19 feet, and (4) the Storage Cask tip-over event. As discussed in Section B.1.4, the probability of a single element failure through the thickness of the shell is not the same as the probability of a breach of the confinement boundary. However, for the purpose of this PRA, the probability of a single element failure through the thickness will be conservatively equated to the probability of a breach.

Table B.9: Summary of the Probability of MPC Weld Crack Initiation for Various Impact Events

Event Scenario	Impact Surface (Target)	Drop Height (feet)	Probability of Weld Crack Initiation
Transfer Cask Vertical Drop	Concrete Floor	5	< 0.000001
		40	0.000360

		70	0.002600
		100	0.019600
	Storage Cask	5	0.000002[1]
		40	0.000014
		80	0.000203
Drop of MPC into Storage Overpack during Transfer Operations	Storage Overpack Pedestal	19	0.282000
Storage Cask Tip-over	Concrete Pad	NA	< 0.000001

[1]This value should be <0.000001. See Table A.4 note 2.

Thermal loads

The creep, limit load, and fracture models were used to analyze the MPC failure probability for the external fire and blocked vent accident scenarios. Table B.10 shows the MPC temperature and pressure conditions for these events.

Under normal steady-state conditions, the bulk MPC internal pressure is 0.565 MPa (82 psi). The MPC temperature varies with axial location as shown in Figure B.12. In this figure, height is measured from the base of the storage overpack such that the bottom of the helium gas and fuel rods are at a height of 0.67 m (2.2 ft). The minimum temperature of 73°C (163°F) occurs at the shell to baseplate weld at the bottom of the MPC. The maximum MPC temperature of 180°C (356°F) is located at the top of the MPC. Even though the axial weld temperature varied between these two extremes, the failure analyses assumed a uniform temperature equal to the maximum value. Even if these conditions were maintained for the full 20 year license period of the cask, the failure analysis shows that no MPC failures are expected.

If the storage cask was exposed to an external fire for 3 hours resulting from a Gulfstream IV aircraft crash, the MPC pressure will increase to 0.634 MPa (92 psi). However, as mentioned in section B.1.2, a credible fire scenario will be much less than 30 minutes. As a result, the values resulting from the 3 hours fire analysis are very conservative. The MPC temperature will also increase as shown in Table B.10 and Figure B.12. Since creep failure is a time at temperature phenomenon, it was assumed that the 3 hour fire occurred after the 20 year license period of the cask. Even under these conditions, the failure analysis shows that no MPC failure is expected.

Table B.10: MPC Temperature and Pressure Conditions Following External Fires and Blocked Vent Scenarios

Quantity, **Units**: **SI (U.S.)**	Normal Steady State Conditions	3 Hour Fire	100% Vent Blockage, No Fuel Rupture
Internal Pressure, **MPa (psi)**	0.565 (82)	0.634 (92)	0.745 (108)
Maximum Temperature in Axial Weld, **°C (°F)**	172 (342)	352 (666)	283 (542)
Temperature of Circumferential Weld, **°C (°F)**	133 (271)	331 (628)	279 (534)
Temperature of Shell to Baseplate Weld, **°C (°F)**	73 (163)	335 (635)	206 (403)

If all four cooling vents become blocked, the MPC temperatures will increase to new steady state values shown in Table B.10 and Figure B.12. The bulk MPC pressure would become 0.745 MPa (108 psi). The results in Appendix C (Response of Fuel to Loads) show that for vent blockage none of the fuel within the cask is expected to fail.

References

1. HOLTEC International, "HI-STORM Final Safety Analysis Report," HI-2002444, Revision 1, September 6, 2002.

2. American Iron and Steel Institute, "High-Temperature Characteristics of Stainless Steels," Nickel Develop Institute Publication No 9004.

3. Smith, G.V., "An Evaluation of the Yield, Tensile, Creep, and Rupture Strengths of Wrought 304, 316, 321, and 347 Stainless Steels at Elevated Temperatures," ASTM Data Series DS 5S2, American Society for Testing and Materials, 1969.

4. Klueh, R.L., and Canonico, D.A., "Elevated Temperature Tensile Strength and Microstructure of a Weld-Overlaid Type 304 Stainless Steel Forging," Symposium on Elevated Temperature Properties of Austenitic Stainless Steels, June 24-28, 1974.

5. National Research Institute for Metals, "Data Sheets on the Elevated-Temperature Properties for Base Metals, Weld Metals, and Welded Joints of 18Cr-8Ni Stainless Steel Plates," NRIM Creep Data Sheet No 32A, Tokyo Japan, 1995.

6. Vacari, J.A., "Standard Wrought Austenitic Stainless Steels," Materials Engineering, December, 1974.

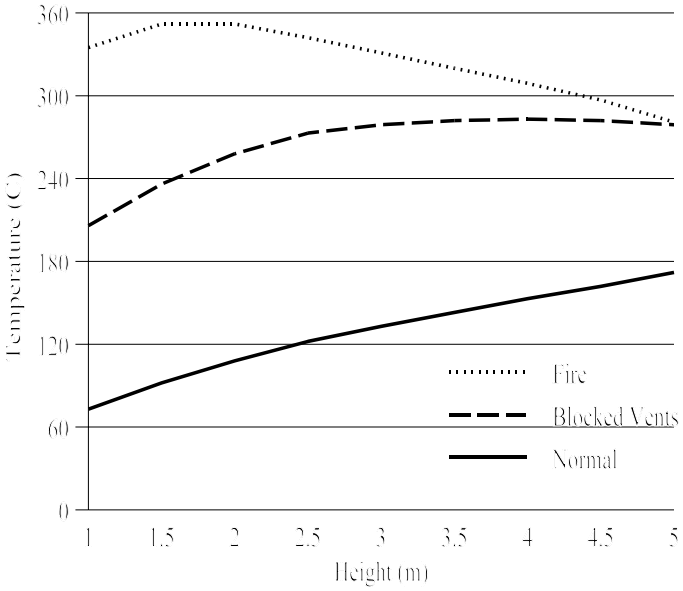

Figure B.12: MPC Wall Temperatures as a Function of Axial Height

7. Conway, J.B., “Stress-Rupture Parameters: Origin, Calculation and Use,” Gordon and Breach, Science Publishers, New York, 1969.

8. Chapman, O.J.V., “Simulation of Defects in Weld Construction,” Reliability and Risk in Pressure Vessels and Piping, PVP-Vol. 251, pp. 81-89, American Society of Mechanical Engineers, 1993.

9. Chapman, O.J.V., Khaleel, M.A. and Simonen, F.A. “A Simulation Model for Estimating Probabilities of Defects in Welds,” ASME PVP Vol. 323, pp 375-391, Fatigue and Fracture, 1996, Volume 1, American Society of Mechanical Engineers

10. Chapman, O.J.V., and Simonen, F.A. “RR-PRODIGAL: Model for Estimating the Probabilities of Defects in Reactor Pressure Vessel Welds,” NUREG/CR-5505, Nuclear Regulatory Commission, Washington DC, 1998.

11. Chapman, O.J.V., M.A. Khaleel, Simonen, F.A., and Harris, “A Method for Estimating the Probabilities of Defects in Piping Welds,” ASME PVP Vol 386, pp. 127-144, Probabilistic and Environmental Aspects of Fracture and Fatigue, 1999.

12. Schuster, G.J., Doctor, S.R., and Simonen, F.A., “A Methodology for Determining Fabrication Flaws in a Reactor Pressure Vessel,” Proceedings of ASME-JSME International Conference on Nuclear Engineering, 1996, ICONE4, Volume 1, Part A, Basic Technological Advances, pp. 187-194, American Society of Mechanical Engineers.

13. Schuster, G.J., Doctor, S.R., Pardini, A.F., “Validation of Reactor Pressure Vessel Fabrication Flaws,” Electric Power Research Institute, Proceedings of NDE Damage Assessment Workshop, October 6-7, 1997, La Jolla, California.

14. Majumdar, S., Shack, W.J., Diercks, D.R., Mruk, K., Franklin, J., and Knoblich, L., “Failure Behavior of Internally Pressurized Flawed and Unflawed Steam Generator Tubing at High Temperatures Experiments and Comparison with Model Predictions,” NUREG/CR-6575, March, 1998.

15. Holt, J., Mindlin, H. And Ho, C., “Structural Alloys Handbook,” 1996 Edition, CINDAS/Purdue University.

16. Peckner, D. and Bernstein, I., “Handbook of Stainless Steel,” McGraw-Hill.

17. “Atlas of Stress-Strain Curves,” Second Edition, American Society of Metals.

18. Ward, A., and Blackburn, L., “elevated Temperature Tensile Properties of Weld-Deposited Austenitic Stainless Steels,” ASME Journal of Engineering Materials and Technology, July, 1976.

19. Stoner, K., Sindelar, R. And Caskey, G., “Reactor Materials Program - Baseline Material Property Handbook - Mechanical Properties of 1950's vintage Stainless Steel Weldment Components,” TN: 89-023-A-1, Westinghouse Savannah River Company, WSRC-TR-91-10, April 1991.

20. Lee, W., Lin, C., Liu, C. And Cheng, C., “The Effects of Strain Rate and Welding Current Mode on the Dynamic Impact Behavior of Plasma-Arc-Welded 304L Stainless Steel,”

21. Davis, E. And Connelly, F., “Stress Distribution and Plastic Deformation in Rotating Cylinders of Strain-Hardening Materials,” ASME Journal of Applied Mechanics, March 1959.

22. Manjoine, M., “Ductility Indices at Elevated Temperature,” Transactions of ASME, April 1975.

23. Manjoine, M., “Creep-Rupture Behavior of Weldments,” Welding Journal - Research Supplement, V61, N2, February 1982.

24. Singh, K. P., Zhai, J., “Multi-Purpose Canister: A Bulwark of Safety in the Post - 9/11 Age,” International High Level Radioactive Waste Management Conference, Las Vegas, NV, 2003.

This page is intentionally blank.